Full flex-grid asynchronous multiplexing demonstrated with Nyquist pulse-shaping

P. C. Schindler,[1,*] R. Schmogrow,[1,2,3] S. Wolf,[1] B. Baeuerle,[1,2] B. Nebendahl,[4] C. Koos,[1,5] W. Freude,[1,6] and J. Leuthold[1,2,5,7]

[1]*Institute of Photonics and Quantum Electronics (IPQ), Karlsruhe Institute of Technology (KIT), Karlsruhe, Germany*
[2]*Institute of Electromagnetic Fields (IEF), ETH Zurich, Zurich, Switzerland*
[3]*Now with: Infinera Corp., Sunnyvale, CA, USA*
[4]*Agilent Technologies, Boeblingen, Germany*
[5]*Institute of Microstructure Technology (IMT), Karlsruhe Institute of Technology (KIT), Karlsruhe, Germany*
[6]*w.freude@kit.edu*
[7]*juergleuthold@ethz.ch*
[*]*philipp.schindler@kit.edu*

Abstract: We demonstrate full flex-grid operation with Nyquist frequency division multiplexing. The technique supports high spectral efficiency, asynchronous operation of channels, variable channel loading with different modulation formats and dynamic bandwidth allocation. Data from different sources with different bit and symbol rates are encoded onto electrical Nyquist pulses with different electrical subcarrier frequencies, and then transmitted optically. We give details on the transceiver design with digital signal processing and investigate the implementation penalty as a function of several design parameters such as limited filter length and effective number of bits. Finally, experiments are performed for receivers with direct detection, intradyne and remote heterodyne reception.

OCIS codes: (060.4510) Optical communications; (060.1660) Coherent communications.

References and links

1. R. Schmogrow, D. Hillerkuss, S. Wolf, B. Bäuerle, M. Winter, P. Kleinow, B. Nebendahl, T. Dippon, P. C. Schindler, C. Koos, W. Freude, and J. Leuthold, "512QAM Nyquist sinc-pulse transmission at 54 Gbit/s in an optical bandwidth of 3 GHz," Opt. Express **20**(6), 6439–6447 (2012).
2. Y. Koizumi, K. Toyoda, M. Yoshida, and M. Nakazawa, "1024 QAM (60 Gbit/s) single-carrier coherent optical transmission over 150 km," Opt. Express **20**(11), 12508–12514 (2012).
3. W. Shieh, H. Bao, and Y. Tang, "Coherent optical OFDM: theory and design," Opt. Express **16**(2), 841–859 (2008).
4. T. Pollet, M. Van Bladel, and M. Moeneclaey, "BER sensitivity of OFDM systems to carrier frequency offset and Wiener phase noise," IEEE Trans. Commun. **43**(2/3/4), 191–193 (1995).
5. G. Bosco, A. Carena, V. Curri, P. Poggiolini, and F. Forghieri, "Performance limits of Nyquist-WDM and CO-OFDM in high-speed PM-QPSK systems," IEEE Photon. Technol. Lett. **22**(15), 1129–1131 (2010).
6. D. Hillerkuss, R. Schmogrow, M. Meyer, S. Wolf, M. Jordan, P. Kleinow, N. Lindenmann, P. Schindler, A. Melikyan, X. Yang, S. Ben-Ezra, B. Nebendahl, M. Dreschmann, J. Meyer, F. Parmigiani, P. Petropoulos, B. Resan, A. Oehler, K. Weingarten, L. Altenhain, T. Ellermeyer, M. Moeller, M. Huebner, J. Becker, C. Koos, W. Freude, and J. Leuthold, "Single-laser 32.5 Tbit/s Nyquist WDM transmission," J. Opt. Commun. Netw. **4**(10), 715–723 (2012).
7. J. C. Cartledge, J. D. Downie, J. E. Hurley, A. S. Karar, Y. Jiang, and K. Roberts, "Pulse shaping for 112 Gbit/s polarization multiplexed 16-QAM signals using a 21 GSa/s DAC," Opt. Express **19**(26), B628–B635 (2011).
8. R. Schmogrow, S. Wolf, B. Baeuerle, D. Hillerkuss, B. Nebendahl, C. Koos, W. Freude, and J. Leuthold, "Nyquist frequency division multiplexing for optical communications," in *Proc. Conf. Laser Electro-Optics* (2012), paper CTh1H.2.
9. R. Schmogrow, M. Meyer, P. C. Schindler, B. Nebendahl, M. Dreschmann, J. Meyer, A. Josten, D. Hillerkuss, S. Ben-Ezra, J. Becker, C. Koos, W. Freude, and J. Leuthold, "Real-time Nyquist signaling with dynamic precision and flexible non-integer oversampling," Opt. Express **22**(1), 193–209 (2014).
10. R. Schmogrow, M. Winter, M. Meyer, D. Hillerkuss, S. Wolf, B. Baeuerle, A. Ludwig, B. Nebendahl, S. Ben-Ezra, J. Meyer, M. Dreschmann, M. Huebner, J. Becker, C. Koos, W. Freude, and J. Leuthold, "Real-time Nyquist pulse generation beyond 100 Gbit/s and its relation to OFDM," Opt. Express **20**(1), 317–337 (2012).
11. J. Geyer, C. Fludger, T. Duthel, C. Schulien, and B. Schmauss, "Efficient frequency domain chromatic dispersion compensation in a coherent polmux QPSK-receiver," in *Optical Fiber Communication Conference* (2010), paper OWV5.

#206966 - $15.00 USD Received 27 Feb 2014; revised 21 Apr 2014; accepted 21 Apr 2014; published 29 Apr 2014

12. A. V. Oppenheim, R. W. Schafer, and J. R. Buck, *Discrete-Time Signal Processing* (Prentice-Hall, 1989), Vol. 2.
13. R. Schmogrow, B. Nebendahl, M. Winter, A. Josten, D. Hillerkuss, S. Koenig, J. Meyer, M. Dreschmann, M. Huebner, C. Koos, J. Becker, W. Freude, and J. Leuthold, "Error vector magnitude as a performance measure for advanced modulation formats," IEEE Photon. Technol. Lett. **24**(1), 61–63 (2012).
14. R. Schmogrow, B. Nebendahl, M. Winter, A. Josten, D. Hillerkuss, S. Koenig, J. Meyer, M. Dreschmann, M. Huebner, C. Koos, J. Becker, W. Freude, and J. Leuthold, "Corrections to: Error vector magnitude as a performance measure for advanced modulation formats," IEEE Photon. Technol. Lett. **24**(23), 2198 (2012).
15. R. Essiambre, G. Kramer, P. Winzer, G. Foschini, and B. Goebel, "Capacity limits of optical fiber networks," J. Lightwave Technol. **28**(4), 662–701 (2010).
16. M. Sjödin, P. Johannisson, H. Wymeersch, P. A. Andrekson, and M. Karlsson, "Comparison of polarization-switched QPSK and polarization-multiplexed QPSK at 30 Gbit/s," Opt. Express **19**(8), 7839–7846 (2011).
17. B. Spinnler, "Equalizer design and complexity for digital coherent receivers," IEEE J. Sel. Top. Quantum Electron. **16**(5), 1180–1192 (2010).
18. R. Bonk, T. Vallaitis, J. Guetlein, C. Meuer, H. Schmeckebier, D. Bimberg, C. Koos, W. Freude, and J. Leuthold, "The input power dynamic range of a semiconductor optical amplifier and its relevance for access network applications," IEEE Photon. J. **3**(6), 1039–1053 (2011).
19. P. C. Schindler, R. Schmogrow, M. Dreschmann, J. Meyer, I. Tomkos, J. Prat, H.-G. Krimmel, T. Pfeiffer, P. Kourtessis, A. Ludwig, D. Karnick, D. Hillerkuss, J. Becker, C. Koos, W. Freude, and J. Leuthold, "Colorless FDMA-PON with flexible bandwidth allocation and colorless, low-speed ONUs [invited]," J. Opt. Commun. Netw. **5**(10), A204–A212 (2013).

1. Introduction

Asynchronously multiplexing various tributaries on a flexible grid allows for transmission at highest spectral efficiency (SE) even when traffic patterns change. In the past, most efforts in increasing the SE were concentrated on reducing guard bands (GB) in wavelength division multiplexed (WDM) schemes and on applying advanced modulation formats such as *M*-ary quadrature amplitude modulation (QAM) [1,2]. Pulse-shaping as a form of digital signal processing (DSP) can help increasing the spectral efficiency (SE) further, .As an example, orthogonal frequency division multiplexing (OFDM) [3] has emerged as a promising candidate for both, long-haul and access networks. In OFDM, a channel consists of a group of sinc-shaped overlapping equidistant spectra with identical width. And indeed, OFDM offers a high SE and dynamic bandwidth allocation (DBA). Yet, the granularity in OFDM is limited by the number of subcarriers (SC) and with this by the processing capabilities. In addition, the data on the frequency-locked SCs need to be transmitted in synchronism, and even small deviations of the SC frequencies from an equidistant spacing cannot be tolerated to avoid severe crosstalk [4]. Tolerance towards synchronicity can for instance be obtained by introducing a cyclic extension of the symbols (cyclic prefix, CP). However, a CP reduces the symbol rate and hence the SE. Recently, Nyquist-WDM was introduced [5,6] using modulated sinc-shaped Nyquist pulses having a rectangular spectrum [7].

In this paper, we propose electrical Nyquist frequency division multiplexing (NFDM) and demonstrate it with up to 5 independent SCs [8]. All SCs are encoded with Nyquist sinc-shaped pulses, resulting in rectangular non-overlapping spectra each representing one electrical NFDM channel. Like OFDM, NFDM supports variable channel loading, i.e., choosing the channels modulation formats individually. However, NFDM offers truly independent SCs offering flexible symbol rate per channel [9]. As SC bands are near the fundamental Nyquist limit, no guard bands are required. Synchronization of different transmitters is not required thanks to the non-overlapping spectra. In addition, the narrow shape of each SC offers a high chromatic dispersion (CD) and polarization mode dispersion (PMD) tolerance inside each electrical SC band. As an advantage, no CP is needed for dispersion compensation. Due to the versatility of the concept, both constant and flexible electrical subcarrier grids are supported.

The paper is organized as follows. In Section 2, the DSP transceiver design is discussed. The impact of parameters such as filter length and resolution of digital-to-analog converters (DAC) is investigated for 16QAM NFDM signals, which are then transmitted optically. In Section 3 we demonstrate a five-channel 16QAM flex-grid operation. Finally, in Section 4 we measure the error vector magnitude (EVM) and the bit error ratio (BER) as a function of the optical signal-to-noise ratio (OSNR) for signals with electrical quadrature phase shift keying

#206966 - $15.00 USD Received 27 Feb 2014; revised 21 Apr 2014; accepted 21 Apr 2014; published 29 Apr 2014

(QPSK) and electrical 16QAM using optical receivers with direct detection, intradyne and remote heterodyne reception.

2. Transceiver design: digital signal processing

We begin with a discussion of the NFDM transceiver and its DSP implementations in time and frequency domain, and comment on the respective advantages of each approach.

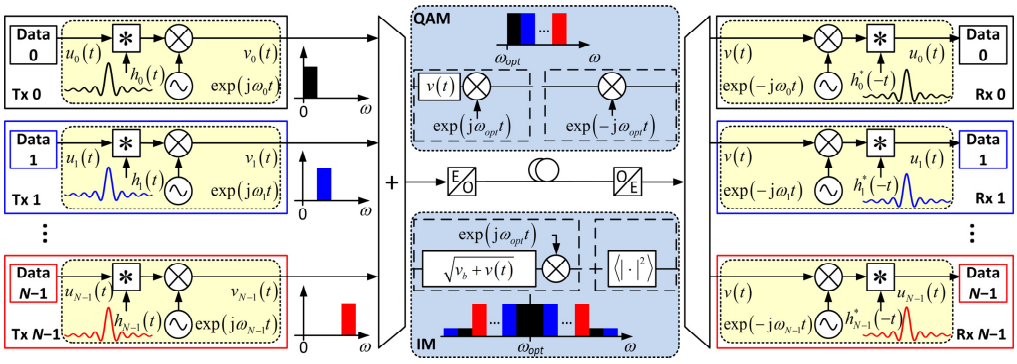

Fig. 1. Schematic of the NFDM link. A number of N Nyquist pulse transmitters (Tx) with electrical subcarrier (SC) frequencies $f_n = \omega_n/(2\pi)$ define N channels of the NFDM signal. A complex mixer modulates each SC with complex data shaped by a filter with sinc-shaped impulse response $h_n(t)$. The electrical NFDM signal is formed by a superposition of all modulated SCs. An electro-optic (E/O) converter mixes the data $v(t)$ onto an optical carrier. This can be done by either I/Q-modulation, see upper inset "QAM", or by intensity modulation (bias v_b), see bottom inset "IM". After back-to-back transmission, an opto-electric (O/E) converter recovers the electrical signal $v(t)$, either by homodyne reception with a local oscillator $\exp(-\mathrm{j}\omega_{opt}t)$, or by direct detection $\langle|\cdot|^2\rangle = v_v + v(t)$. After O/E conversion, the electrical signal $u_n(t)$ is received by N homodyne receivers for the respective subcarriers. Matched filters with sinc-shaped impulse responses $h_n^*(-t) = h_n(t)$ avoid inter-channel interference (ICI).

The schematic NFDM transceiver design is depicted in Fig. 1. The complex data signals $u_n(t)$ are fed to a number of N Nyquist pulse transmitters (Tx) comprising pulse-shapers. The employed impulse response is a sinc-function in time with the symbol duration T_s

$$h(t) = \mathrm{sinc}\left(\frac{t}{T_s}\right) = \frac{\sin(\pi t/T_s)}{\pi t/T_s}. \tag{1}$$

Complex mixers with local oscillators (LO) $\exp(\mathrm{j}\omega_n t)$ perform the up-conversion of complex modulated SC, being tributaries $v_n(t)$ of the electrical NFDM signal

$$v(t) = \sum_{n=0}^{N-1} v_n(t) = \sum_{n=0}^{N-1} u_n(t) * h(t) \exp(\mathrm{j}\omega_n t). \tag{2}$$

The NFDM signal $v(t)$ is electro-optically (E/O) converted by either of two methods, Fig. 1. The complex signal $v(t)$ either modulates an optical carrier $\exp(\mathrm{j}\omega_{opt}t)$ by I/Q-modulation, resulting in a quadrature-amplitude modulated optical field (QAM, upper inset in Fig. 1),

$$E(t) = v(t)\exp(\mathrm{j}\omega_{opt}t). \tag{3}$$

#206966 - $15.00 USD Received 27 Feb 2014; revised 21 Apr 2014; accepted 21 Apr 2014; published 29 Apr 2014

Alternatively, a properly biased ($v_b > 0$) signal $|v(t)| \le v_b$ linearly modulates the optical intensity $\left\langle |E(t)|^2 \right\rangle$, see lower inset "IM" in Fig. 1. The notation $\langle \cdot \rangle$ indicates averaging over a few optical periods. We find

$$E(t) = \sqrt{v_b + v(t)} \exp\left(\mathrm{j}\omega_{opt} t\right). \tag{4}$$

After transmission, an opto-electric (O/E) converter recovers the electrical signal $v(t)$ with a complex mixer and a local oscillator $\exp\left(-\mathrm{j}\omega_{opt} t\right)$. Alternatively, direct detection $\left\langle |E(t)|^2 \right\rangle$ is employed. The NFDM is distributed to a set of N receivers (Rx) with complex mixers and local oscillators adjusted for the desired subcarrier. The N receivers (Rx) implement matched filters with sinc-shaped impulse responses. Finally, the data are decoded in each channel.

In the following, we discuss the Tx and Rx implementation in the digital domain using a time domain and frequency domain approach.

2.1 Time domain DSP

The transmitter schematic for time domain (TD) digital signal processing (DSP) of N NFDM channels is depicted in Fig. 2. A time domain DSP implementation is interesting for applications with short, numerically inexpensive filters $h(t)$ with a few taps only [9].

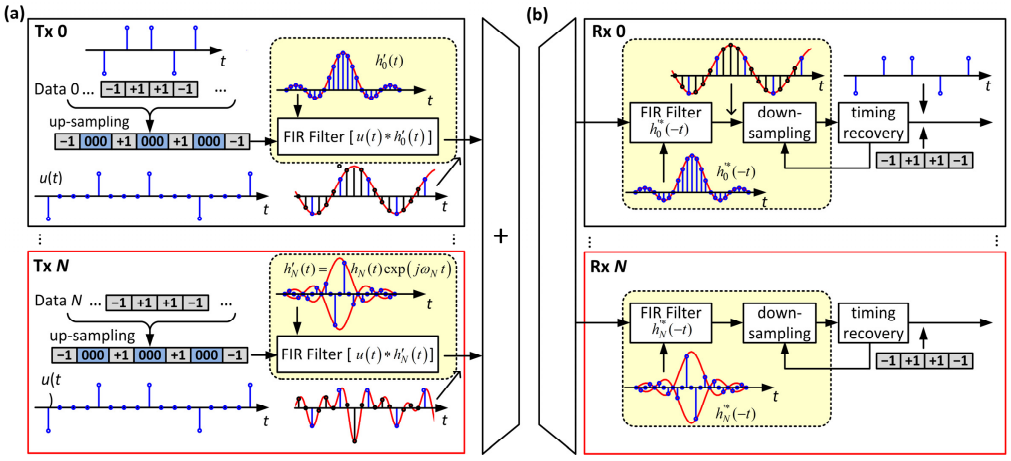

Fig. 2. Nyquist time domain digital signal processing (DSP). In contrast to Fig. 1 we choose $\omega_0 = 0$. (a) Transmitters: Input data are up-sampled by a factor q through inserting $q - 1$ zeros in-between data samples. The signal is then convolved with a Nyquist sinc-shaped impulse response $h_n(t)$ and simultaneously mixed with the subcarrier ω_n resulting in an impulse response h_n', see Appendix. (b) Receivers: The input signal feeds matched FIR filters having impulse responses $h_n'^*(-t)$ corresponding to the ones of the Tx. After down-sampling and timing recovery [10] the data are recovered.

The data to be transmitted are represented by time-discrete samples, Fig. 2(a). We describe the process for real-valued data coefficients −1 and + 1 only, but an extension to complex data is easily possible. The data are mapped on one out of N electrical subcarriers, the largest frequency of which determines the minimum sampling rate for all SC channels. The data are represented by one sample per symbol (SPS). For generating a guard band between adjacent Nyquist spectra, we up-sample by a factor of q (here: q = 4) by inserting

#206966 - $15.00 USD Received 27 Feb 2014; revised 21 Apr 2014; accepted 21 Apr 2014; published 29 Apr 2014

$q-1$ zeroes in-between adjacent samples. The up-sampling factor q determines the spectral width and, for a given sampling rate, also the maximum number of NFDM channels.

For TD pulse shaping, finite-duration impulse response (FIR) filters are employed [10]. First the input signal $u(t)$ is convolved with the filter's impulse response $h(t)$. The filter output is mixed with each Tx's subcarrier (SC). For avoiding run-time multiplications, filtering and SC mixing can be combined in one pre-calculated module which is stored in a look-up table, see Appendix.

The TD-NFDM receiver concept is schematically depicted in Fig. 2(b). At the input, matched filters select the channel of interest and simultaneously perform a down-conversion, see Appendix. In a next step, the signal is down-sampled with a clock recovery method as described in [10], and data are recovered.

2.2 Frequency domain DSP

As an alternative to TD processing, frequency domain (FD) DSP can improve the resource utilization especially for long filter impulse responses [9].

Performing the convolution in the frequency domain is referred to as fast convolution. First, a m_n-point fast Fourier transform (FFT) converts a block of m_n TD data (here ± 1) to the frequency domain, see Fig. 3(a). The output is zero-padded by $M - m_n$. for (M / m_n)-fold oversampling. Each channel is then shifted to the position of its respective SC. Addition of all channel spectra yields the aggregate signal spectrum that is transferred to the TD by an M-point IFFT. The output is parallel-serial converted and transmitted.

At the Rx the compound signal is serial-parallel converted and transformed to the frequency domain by an M-point FFT, see Fig. 3(b). The filter $H_n(f)$ selects the m_n points corresponding to the chosen channel out of the M inputs. A subsequent m_n-point IFFT recovers the data using a clock recovery [10] to synchronize the IFFT with the FFT.

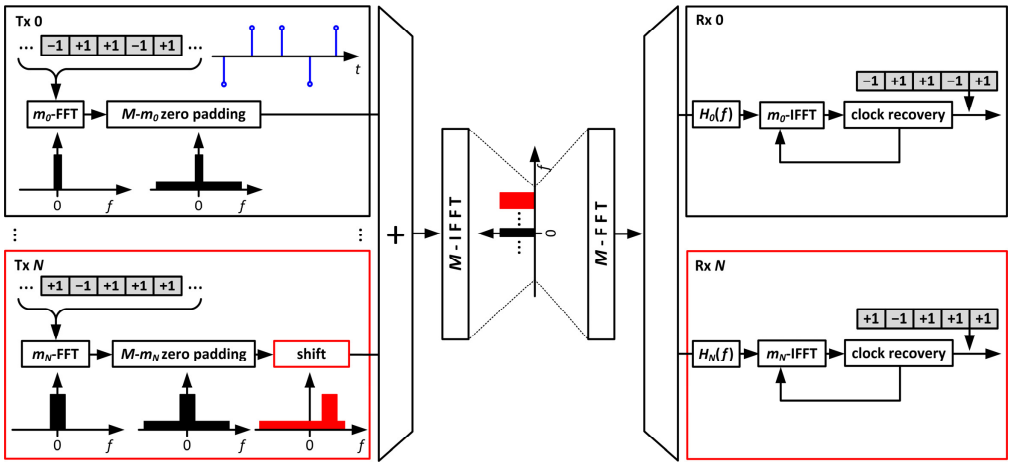

Fig. 3. Nyquist frequency domain digital signal processing (DSP) for NFDM. (a) The Tx maps a block of m_n complex TD data (here: ± 1) to the input of an m_n-point FFT. Symmetrical insertion of $M - m_n$ zeroes (zero padding) corresponds to (M / m_n)-fold oversampling. The m_n-point FFT is shifted to the proper SC position inside the M-point array. The shifted spectra are added and input to an M-point IFFT. These TD output data blocks are then parallel-to-serial converted and transmitted. (b) After a serial-to-parallel conversion, the Rx M-point FFT transforms the compound TD signal blockwise to the frequency domain. The proper channel is selected by an M-point filter $H_n(f)$, which selects at its output only the m_n points corresponding to the chosen channel. Next a m_n-point IFFT recovers the modulation coefficients. A clock recovery [9] synchronizes each m_n-point IFFT with the M-point FFT.

The resource tradeoff between time domain and frequency domain DSP with respect to different filter lengths has been investigated in [9] and [11]. However, a fast convolution [12] is performed block-wise with FFT-IFFT transform pairs using the overlap-and-add or overlap-

#206966 - $15.00 USD Received 27 Feb 2014; revised 21 Apr 2014; accepted 21 Apr 2014; published 29 Apr 2014

and-save method. This implies some processing overhead, which has not been mentioned when comparing FD-DSP and TD-DSP.

2.3 Implementation penalties due to limited filter length and DAC resolution

So far, ideal non-causal signals have been assumed, leading to perfectly rectangular channel spectra without any inter-channel interference (ICI). However, in a real-word implementation at least two compromises need to be made.

First, the ideal sinc-shaped filter impulse response $h(t)$ needs to be approximated with a discrete FIR filter having a finite number R of coefficients, thus leading to a finite-length impulse response of length L. The resulting NFDM channel spectra, therefore, deviate from an ideal rectangle [10].

In order to experimentally investigate the effect of filter order R on the observed ICI, we use the setup depicted in Fig. 4 and compare the outcome to simulations. An Agilent M9180A arbitrary waveform generator (AWG) with 12 bit resolution and a sampling rate of 12 GSa/s stores pre-computed NFDM signals comprising five channels of equal bandwidth. All channel centers are spaced by the Nyquist bandwidth of the channels, so that guard bands do not exist. The electrical outputs of the AWG drive an optical I/Q-modulator that modulates an external cavity laser (ECL). The center wavelength of this ECL is set to 1550 nm, and the linewidth is specified as 100 kHz. An erbium-doped fiber amplifier (EDFA) amplifies the optical signals. The Agilent N4391A optical modulation analyzer (OMA) coherently receives the NFDM signals. The OMA comprises two 90° optical hybrids (one for each polarization) and two real-time oscilloscopes with two 32 GHz channels each. The oscilloscopes sample at a maximum rate of 80 GSa/s.

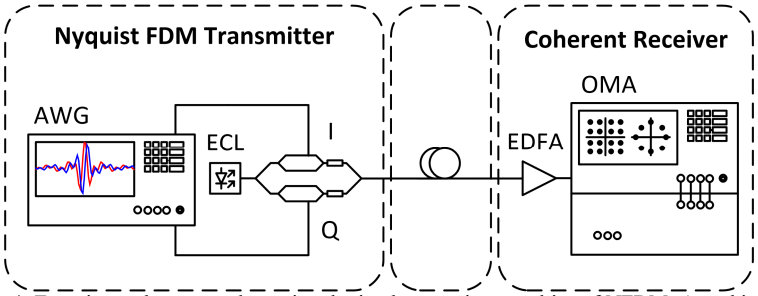

Fig. 4. Experimental setup to determine the implementation penalties of NFDM. An arbitrary waveform generator (AWG) drives an optical I/Q-modulator. NFDM data are encoded on an external cavity laser (ECL), the output of which is amplified by an erbium doped fiber amplifier (EDFA) and coherently received by an optical modulation analyzer (OMA).

In order to evaluate the influence of ICI as a function of filter length, we transmit de-correlated 1.5 GBd 16QAM data in five adjacent zero-guard band NFDM channels, which are consecutively numbered from 0 to 4. We record the error vector magnitude (EVM) [13,14] for the middle channel 2. The length L of the filter's impulse response depends on the filter order R, the oversampling factor q, and the symbol duration T_s [9],

$$L = RT_S/q. \tag{5}$$

The results are shown in Fig. 5(a). Simulations (black) and measurements (blue) coincide except for an EVM implementation penalty of 1 percentage point. This stems from the fact that simulations are performed without any added noise to isolate the effect of ICI. Insets of Fig. 5(a) show two constellation diagrams for $L = 64\ T_s$ and $L = 512\ T_s$, respectively.

Second, we investigate the influence of the digital-to-analog converter (DAC) resolution on the achievable signal quality. Figure 5(b) depicts the outcome of simulations (left) and measurements (right). We have computed all NFDM waveforms using floating point double precision (52 bit significant, 1 hidden bit, an 11 bit exponent, and a sign bit) before reducing the number of quantization steps to the resolution listed on the horizontal axis of Fig. 5(b). From simulations and measurements we see that the use of long filters tends to require higher

#206966 - $15.00 USD Received 27 Feb 2014; revised 21 Apr 2014; accepted 21 Apr 2014; published 29 Apr 2014

DAC resolutions. However, DACs with a physical resolution of at least 6 bit suffice without compromising the signal quality significantly.

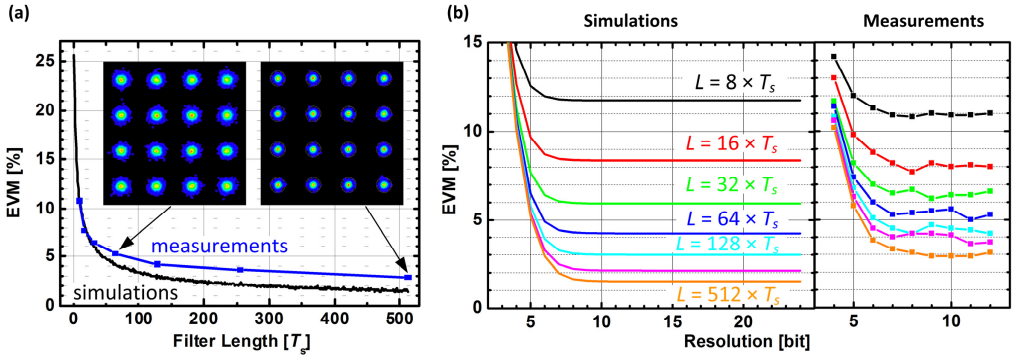

Fig. 5. Effect of penalties due to a limited filter length and DAC resolution as for the middle channel in a 5 channel transmission. (a) Linear inter-channel crosstalk for transmission of a 1.5 GBd 16QAM NFDM signal. The amount of crosstalk is specified by the error vector magnitude (EVM) for both simulations (black) and measurements (blue). As expected, an increase of the impulse response length L confines the spectrum more closely to the Nyquist band, and therefore reduces the observed crosstalk. We see an EVM implementation penalty of 1 percentage point when comparing simulations without noise to actual measurements. The insets show two constellation diagrams for two different impulse response lengths. (b) Influence of DAC resolution of the NFDM transmitter on the achievable EVM for NFDM channels generated with filters of different lengths. Signals are computed with double precision (64 bit) and then reduced to the specified resolution. In tendency, a higher resolution is required when increasing the filter's response length. However, a DAC with 6 bit resolution suffices without compromising the signal quality. (b) left: Simulation. (b) right: Measurement.

3. Flex-grid operation

A distinct feature of NFDM is the support of so-called flex-grid operation, i. e., the NFDM channel position and bandwidth can be chosen at will. In order to demonstrate this capability an aggregate NFDM signal is created consisting of five individual channels. We first assess the back-to-back performance at high OSNR and demonstrate the feasibility of flex-grid operation within an experiment using the setup of Fig. 4. We then simulate the performance and depict the bit error ratio (BER) as a function of the signal-to-noise power ratio (SNR) per bit [15].

For the experiment and the simulation, the DSP transceivers described in Section 2.1 were implemented using Matlab. Each of the five channels carries de-correlated pseudo-random binary sequences (PRBS) mapped with either QPSK or 16QAM. The measured channel spectra transporting 16QAM signals are depicted in Fig. 6(a) along with their back-to-back constellation diagrams. In order to illustrate the flex-grid feature, the NFDM channels were chosen to have an arbitrary bandwidth and center frequency. The symbol rates are chosen as fraction sof the AWG sampling rate 12 GSa/s: f_s / 15 (black), f_s / 32 (red), f_s / 8 (green), f_s / 16 (blue), and f_s / 10 (cyan). The length of the FIR filter's impulse response in used for pulse shaping is $L = 128 \times T_s$. We see that the performance of the channel depends on its width. The finite length of the filter results in a non-ideal out-of-band suppression and thus in an overlap with neighboring channels. The smaller the channel is, the larger the de-correlated inter-channel interference (ICI) becomes. It can be represented by Gaussian noise and causes the significant increase of the BER for the red channel.

In a next step, the BER of the individual channels as a function of the SNR per bit [14] was determined by simulations. For varying the SNR, additive white Gaussian noise (AWGN) with different power was superimposed to the aggregate NFDM signal. The results for QPSK and 16QAM modulation formats are shown in Fig. 6(b). As expected, the SNR per bit is independent of the channel bandwidth, but depends strongly on the modulation format. The experiment as well as the simulation shows that the properties of all the channels can indeed be chosen independently proving that NFDM offers full flex-grid capability without

#206966 - $15.00 USD Received 27 Feb 2014; revised 21 Apr 2014; accepted 21 Apr 2014; published 29 Apr 2014

significant ICI penalties if appropriate FIR filters are used. Still, measurements and simulations differ due to implementation penalties mainly at the receiver in this measurement, causing the increase of BER for the narrow channels.

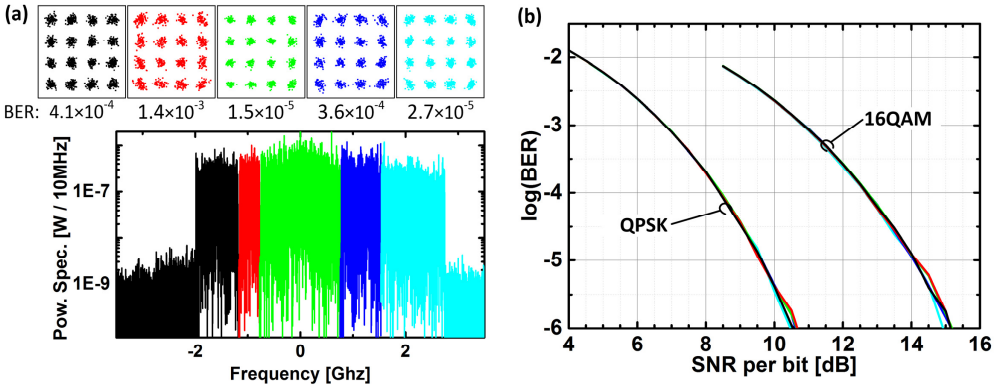

Fig. 6. Flex-grid scenario of five NFDM channels with varying bandwidth for transporting 16QAM signals. (a) Lower graph: Measured compound spectrum with color-coded channel spectra. Upper row: Measured back-to-back constellation diagrams and bit error ratio (BER) with identical color coding as the channel spectra. The order R of the filter's impulse response is set to $R = 128$ ($R + 1 = 129$ taps). The finite filter order causes channel spectra to overlap, introducing ICI, thus channels have varying performance linked to their spectral width. The smallest channels suffer strongest. (b) Simulated bit error ratio (BER) for the five channels for QPSK and 16QAM formats as a function of the SNR per bit [15]. As expected, the different color-coded curves virtually coincide. Implementation penalties mainly at the receiver cause the performance difference between experiment and simulation.

4. Applications

In this subsection we investigate the performance of an NFDM signal with five equal channels for different receiver techniques. First, we investigate the performance using a cost-efficient setup based on intensity modulation with direct detection (IM/DD). As a comparison, an optical coherent receiver is used in Subsection 4.2 for achieving the optimum performance. Last, a combination of direct and optical coherent detection is used, i. e., remote heterodyne reception. Here the optical local oscillator is supplied together with the signal itself by the transmitter and received by a single photodiode.

In the following, the signal quality is determined by the optical signal-to-noise power ratio (OSNR) as well as by signal-to-noise power ratio per bit (SNR per bit, $\mathrm{SNR}_{\mathrm{bit}}$). The OSNR is obtained by measuring the power in the signal with an optical spectrum analyzer (OSA) along with the noise that is averaged over two 0.1 nm wide bins 2 nm above and below the signal. The ratio of the two powers then determines the OSNR. The SNR per bit $\mathrm{SNR}_{\mathrm{bit}}$ is calculated from the OSNR in proportion to the bandwidth B of the signal and the bit rate R_b and the number p of polarization states used for transmission [15]

$$\mathrm{SNR} = \mathrm{OSNR}\frac{25\,\mathrm{GHz}}{pB}, \qquad \mathrm{SNR}_{\mathrm{bit}} = \mathrm{OSNR}\frac{25\,\mathrm{GHz}}{pR_b}. \tag{6}$$

In the case of intensity modulated signals, the optical carrier is not suppressed completely and comprises at least half of the optical power that is measured by the OSA. We thus calculate the power in the optical carrier and correct the measured values accordingly. The actual power in the signal is determined by the peak-to-average power ratio (PAPR) of the signal and the modulation depth with which the modulator was operated.

4.1 Direct detection of NFDM signals

For a direct detection scheme, we generate NFDM modulated optical signals by intensity modulation of the external cavity laser (ECL), see experimental setup in Fig. 7(a). To

#206966 - $15.00 USD Received 27 Feb 2014; revised 21 Apr 2014; accepted 21 Apr 2014; published 29 Apr 2014

overcome the limited capability of our AWG, we employ a Xilinx XCVFX200T field programmable gate array (FPGA) and a high-speed Micram DAC. The FPGA stores pre-computed waveforms and drives the DAC. We used a maximum sampling rate of 25 GSa/s. Image rejection low-pass filters (red) remove image spectra appearing at the DAC output. Although intensity modulated optical fields can be generated using cost-efficient directly modulated lasers (DML), the high signal bandwidth shown here calls for external modulation. To this end we use a single optical Mach-Zehnder modulator (MZM) as opposed to the previous section where an optical I/Q-modulator has been employed. The modulator is biased at its quadrature point where the transfer function between optical intensity and electrical drive signal is approximately linear. A variable optical attenuator (VOA) is used to change the input power to the EDFA and thus to adjust the optical SNR (OSNR). The optical spectrum analyzer (OSA) measures the OSNR and assesses optical noise within a bandwidth of 0.1 nm. The optical power launched onto the photodiode (PD) is kept constant throughout the measurements. The same Agilent real-time oscilloscope, which was used in the previous section, samples the electrical output of the PD. Further processing is performed offline including EVM and BER measurements.

We generate NFDM signals comprising three channels carrying either QPSK or 16QAM data. Each channel operates at a symbol rate of 3.125 GBd (25 GSa/s / q, q = 8), resulting in a bit rate of 18.75 Gbit/s for QPSK and 37.5 Gbit/s for 16QAM. The aggregate signal spectrum, composed of three channels with their complex conjugates, is shown in Fig. 7(b). It shows the spectrum as transmitted through the fiber at the receiver. The overall bandwidth is 6 × 3.125 GHz = 18.75 GHz leading to a spectral efficiency of 1 bit/s/Hz for QPSK and 2 bit/s/Hz for 16QAM, respectively. Since we want to use a direct detection receiver, polarization multiplexing is not feasible, and only real signals can be transmitted. Therefore, Hermitian symmetry must be obeyed, i. e., channels at negative frequencies (lower optical sidebands) must carry the complex conjugate data of their corresponding channels at positive frequencies (upper optical sidebands). Hence only three out of six spectra in Fig. 7(b) are independent.

We vary the OSNR and measure BER and EVM. The equivalent BER calculated from measured EVM (lines) [13,14] and the directly measured BER (squares) for all three independent channels are plotted in Fig. 8. While the OSNR and SNR per bit are determined for the complete signal, the SNR of each individual channel should be different due to the roll-off of the spectrum. We thus give the mean BER over all channels for comparison. As

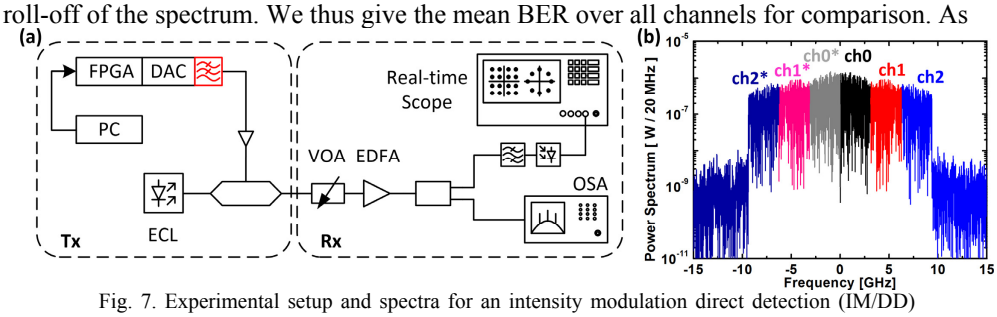

Fig. 7. Experimental setup and spectra for an intensity modulation direct detection (IM/DD) system with NFDM signals. (a) Experimental setup. Pre-computed data from a standard PC are fed to an FPGA followed by a DAC. An electrical low-pass filter removes alias spectra before the amplified electrical signal is fed into an optical Mach-Zehnder modulator (MZM) which is biased at its quadrature point for intensity modulating light from an ECL. The variable optical attenuator (VOA) and the EDFA are used to change the OSNR, which then is measured by the optical spectrum analyzer (OSA). The EDFA output is kept at a constant power level, optically filtered, and then received by a photo-detector (PD). Finally, a real-time oscilloscope records the electrical waveforms after photo-detection. (b) For visualization, we measure the signal with a coherent receiver and depict the resulting electrical aggregate NFDM signal baseband spectrum. The signal comprises three independent channels modulated with QPSK. The channels' symbol rates are 3.125 GBd each. For real modulated signals the spectra must obey a Hermitian symmetry, i. e., spectra at negative frequencies (here: **ch0*, 1*, 2***) are the complex conjugate of spectra at positive frequencies (**ch0, 1, 2**). The performance in later measurements is assessed by direct detection, Fig. 8.

#206966 - $15.00 USD Received 27 Feb 2014; revised 21 Apr 2014; accepted 21 Apr 2014; published 29 Apr 2014

expected, the mean BER corresponds well with the performance of ch1 with an SNR between those of ch0 and ch2. Figure 8(a) shows results for QPSK modulation, while Fig. 8(b) depicts measurements obtained for 16QAM modulated NFDM carriers. The error floor observed in Fig. 8(b) for 16QAM signals at high OSNR stems from the electronic noise of the transmitter and receiver. This noise is below the noise that would normally be picked up from amplification in a long reach system. In any case, one can observe that BER and EVM provide similar results, whereas EVM allows quicker measurements across a larger range.

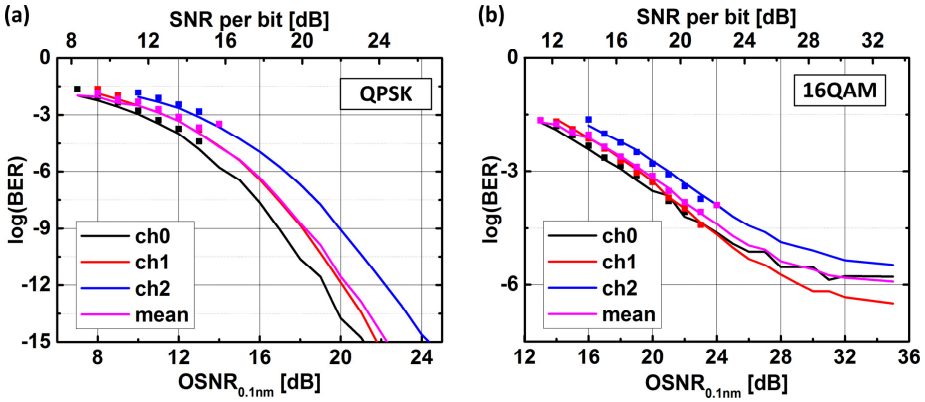

Fig. 8. Experimental results for intensity modulation and direct detection (IM/DD). Measured BER (squares) and equivalent BER derived from measured EVM (lines) as a function of OSNR (reference bandwidth 0.1 nm) and SNR per bit derived from the complete spectrum. All three channels are either modulated with (a) QPSK or (b) 16QAM. All 3 NFDM channels are directly detected with a single PD according to Fig. 7(a). A degradation of the signal quality can be seen when going from ch0 to ch2. This is due to the spectral roll-off also seen in Fig. 7(b). The OSNR is measured for the complete spectrum and we subtracted the power of the optical carrier for comparison. The spectral roll-off causes the channels to have different SNR. For comparison, the mean BER is given in magenta.

4.2 Intradyne reception of NFDM signals

A coherent receiver enables the reception of complex data encoded by an optical I/Q modulator on an optical carrier, Fig. 9(a). In this case, upper and lower optical sidebands are uncorrelated and transmit the real (I) and imaginary parts (Q) of complex NFDM data. As before, the pre-computed signals are stored in two synchronized FPGAs each driving a high-speed Micram DAC. Again, the OSNR is adjusted by a VOA in front of the EDFA. The OMA already described in Section 2.3 coherently receives the NFDM waveforms. Intradyne reception is performed with a second, OMA-internal ECL used as local oscillator. Further processing is performed offline including BER and EVM assessment. The measured aggregate signal spectrum is depicted in Fig. 9(b). The signal comprises five independent channels, each having a symbol rate of 3.125 GBd in a 3.125 GHz optical bandwidth. The resulting data rates are 5 × 3.125 GBd × 2 bit = 31.25 Gbit/s for QPSK, and 62.5 Gbit/s for 16QAM with 4 bit/symbol, respectively. This corresponds to spectral efficiencies of 2 bit/s/Hz (QPSK) and 4 bit/s/Hz (16QAM). The spectral efficiencies can be doubled if polarization division multiplexing (PDM) is applied [16]. As before, the roof-shaped spectral roll-off in Fig. 9(b) is due to the combined electrical frequency responses of Tx and Rx. The roll-off can be compensated at the Tx by a pre-emphasis. Here, we have decided to perform equalization at the Rx instead, for not wasting effective resolution of the DACs to the pre-compensation.

#206966 - $15.00 USD Received 27 Feb 2014; revised 21 Apr 2014; accepted 21 Apr 2014; published 29 Apr 2014

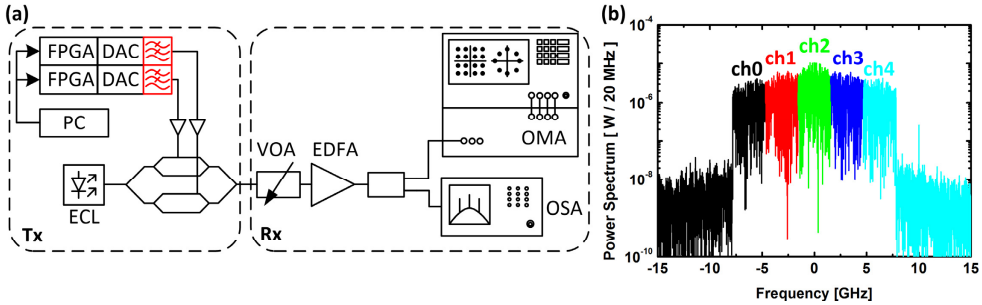

Fig. 9. Experimental setup and spectra for coherently received NFDM signals. (a) Experimental setup. Two synchronized FPGAs store pre-computed NFDM wave-forms. Together with the DACs they again act as an AWG. The amplified outputs drive an optical I/Q-modulator that encodes the waveform onto an ECL. As in the previous setup the OSNR measured by the OSA can be adjusted with a VOA and EDFA pair. The OMA coherently receives and decodes the signals. (b) Measured NFDM signal spectrum comprising 5 independently modulated channels. The modulation format is either QPSK or 16QAM. The spectral roll-off is due to the combined frequency response of Tx and Rx and can be compensated for by means of a pre-emphasis or equalization. Here it will be equalized in the receiver.

The measured BER (squares) and the equivalent BER obtained from EVM measurements (lines) [17] of QPSK modulated NFDM signals at different OSNR are depicted in Fig. 10(a). Channel ch2 located in the center of the spectrum (Fig. 9(b), green spectrum) performs best as expected, because for this channel the highest SNR is observed since it is not significantly suffering from the roll-off. We virtually find the same performance for corresponding channels (i.e. ch1 and ch3 as well as ch0 and ch4) due to the symmetry of the spectrum resulting in the same SNR. When comparing the results from coherent detection to the directly detected signals, we find that coherent detection allows for much lower OSNR for a targeted BER. For 16QAM modulated NFDM signals the BER vs. OSNR results are shown in Fig. 10(b). The OSNR is once more measured for the total signal, but the BER is determined for each channel individually. Due to the roll-off over the spectrum, the SNR of the center channel is higher than that of the outer channels. Thus we give also the mean BER for comparison. The mean BER is nearly identical to the performance of ch2 and ch3, which is once more due to the roll-off of the spectrum. Again measured BER (squares) and equivalent BER (lines) coincide. An increased error floor is observed as compared to the 16QAM BER results with the IM/DD scheme in the previous section, see Fig. 8(b).

The roll-off could be compensated by applying a pre-emphasis. However, this pre-emphasis would reduce the effective number of bits by at least one bit. Taking into account the effective number of bits (ENOB = 5) provided by the DACs, the signal quality would degrade severely by the pre-emphasis according to Fig. 5.

#206966 - $15.00 USD Received 27 Feb 2014; revised 21 Apr 2014; accepted 21 Apr 2014; published 29 Apr 2014

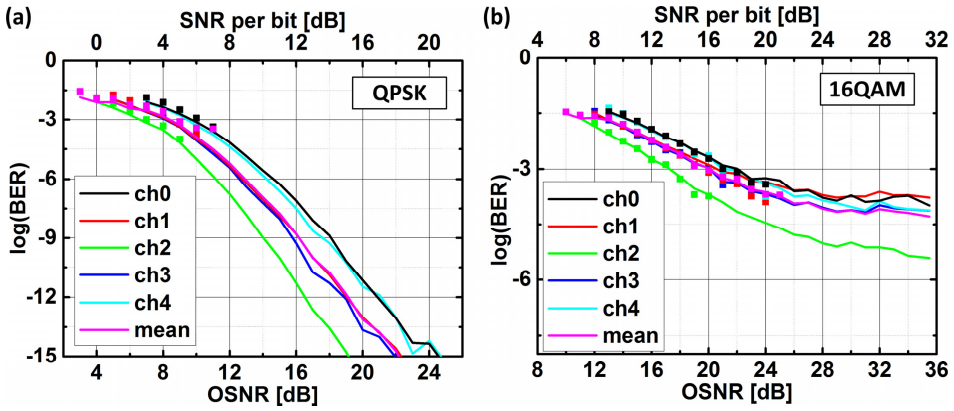

Fig. 10. Intradyne reception of NFDM signals. Measured BER (squares) and BER calculated from measured EVM (lines) as a function of OSNR (reference bandwidth 0.1 nm) and SNR per bit of the complete spectrum. All 5 channels are either modulated with (a) QPSK or (b) 16QAM. The center channel (ch2) performs best as it has the highest SNR, see Fig. 9(b). All measured BER coincide with the equivalent BER obtained from EVM measurements. The OSNR was measured for the complete spectrum, but is not the same for each channel due to the spectral roll-off. The mean BER is depicted as a magenta-colored line for comparison.

4.3 Remote heterodyne reception of NFDM signals

As a third option next to direct and coherent detection, a remote heterodyne setup is investigated as to be seen in Fig. 11(a). To this end we generate two optical carriers from an ECL source by driving an MZM with an 18.75 GHz sinusoidal tone. The two resulting optical carriers with a spacing of 2 × 18.75 GHz = 37.5 GHz are separated using a Finisar WaveShaper. The lower frequency carrier is modulated with the complex NFDM waveform comprising five QPSK modulated channels. The upper frequency carrier is used for remote heterodyne reception. The combined spectrum of signal and auxiliary carrier is schematically shown as an inset in the upper right of Fig. 11(a). The total signal bandwidth that has to be covered by the PD in the Rx is 50 GHz, i.e., twice the signal bandwidth. An EDFA and a VOA control the signal power P_{in} fed to the Rx's semiconductor optical amplifier (SOA). Here we chose an SOA to demonstrate the typical use of such a detection scheme in low-cost applications such as access networks. Finally, the broadband PD converts the optical waveform to an electrical carrier frequency of 37.5 GHz. Complex electrical down-converters select one of the five NFDM channels to be sampled by a 25 GSa/s, 8 GHz real-time oscilloscope. Due to bandwidth limitations we were only able to down-convert two of the five channels (blue and red) centered at electrical carrier frequencies of 31.25 GHz and 34.345 GHz, respectively.

The outcome in terms of measured BER (squares) and equivalent BER from EVM (lines) for different Rx input powers P_{in} is illustrated in Fig. 11(b). At low input powers the signal quality degrades due to thermal noise that is added by the broad-band electrical amplifier required for amplification of the output electrical signal of the PD. Whereas the increasing BER for high input powers ($P_{in} > -12$ dBm) stems from non-linear processes in the SOA [18]. An access network based on NFDM with remote heterodyne reception is investigated in [19].

#206966 - $15.00 USD Received 27 Feb 2014; revised 21 Apr 2014; accepted 21 Apr 2014; published 29 Apr 2014

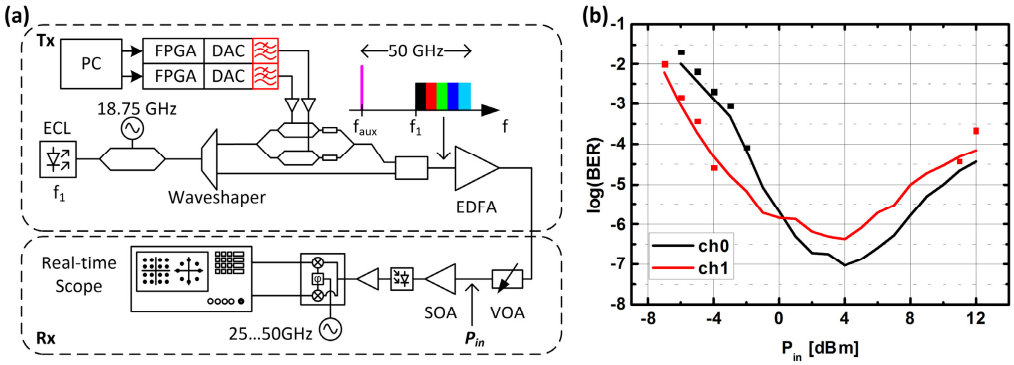

Fig. 11. Experimental setup and results for remote heterodyne detection of QPSK modulated NFDM signals. (a) Experimental setup. Two optical carriers are generated from an ECL using a MZM driven by an 18.75 GHz tone. The carriers are separated with a Finisar WaveShaper and one of the carriers is encoded with NFDM signals whereas the other serves as local oscillator for remote heterodyne detection. The inset shows a schematic of the signal spectrum. The input power P_{in} to the Rx is adjusted and a semiconductor optical amplifier (SOA) boosts the signal that is detected. A single NFDM channel is electrically down-converted and sampled with a real-time oscilloscope. (b) Measured BER (squares) and equivalent BER from EVM (lines) for various levels of Rx input power P_{in}. At low input powers the signal quality is degraded by thermal noise added by the broad-band electrical amplifier after the PD. For high input powers non-linear effects in the SOA limit the signal performance. The smallest BER is observed at input powers $P_{\text{in}} = 4$ dBm.

5. Conclusion

Nyquist frequency division multiplexing offers several advantages over OFDM including the transmission of asynchronous channels with variable bandwidth and channel spacing, such enabling flex-grid operation. We discussed the design of NFDM transceivers with time domain and frequency domain digital signal processing. We further experimentally demonstrated non-coherent and coherent transmission links, and we investigated the performance of channels with QPSK and 16QAM modulated signals.

Appendix

Equivalency of up-converting a shaped sampled signal and up-converting the shaping sampled impulse response

Here we prove the equivalence of mixing a baseband signal $u(t)$ with an oscillator $\exp(\mathrm{j}\omega_n t)$ before applying a filter $h(t)$ on one hand, and of the convolution of the same baseband signal with a frequency shifted filter $h'(t) = h(t)\exp(\mathrm{j}\omega_n t)$ on the other hand:

$$v(t) = \big(u(t) * h(t)\big)\exp(\mathrm{j}\omega_n t), \tag{7}$$

$$v'(t) = u(t) * \big(h(t)\exp(\mathrm{j}\omega_n t)\big). \tag{8}$$

$v(t)$ and $v'(t)$ need to be identical. Using the definition of the convolution, we have to prove

$$\exp(\mathrm{j}\omega_n t)\int_{-\infty}^{+\infty} u(\tau)h(t-\tau)d\tau \overset{?}{=} \exp(\mathrm{j}\omega_n t)\int_{-\infty}^{+\infty} u(\tau)h(t-\tau)\exp(-\mathrm{j}\omega_n \tau)\,d\tau. \tag{9}$$

This would be true for $\exp(\mathrm{j}\omega_n \tau) = 1$ only, i. e. for $\omega_n = 0$. However, for $\omega_n \neq 0$ and for continuous signals this is impossible because $\breve{u}(f - f_v) \neq \breve{u}(f)$,

#206966 - $15.00 USD Received 27 Feb 2014; revised 21 Apr 2014; accepted 21 Apr 2014; published 29 Apr 2014

$$\breve{v}(f) = \int_{-\infty}^{+\infty} \breve{u}(f_1)\breve{h}(f_1)\delta(f - f_1 - f_n)\,\mathrm{d}f_1 = \breve{u}(f - f_n)\breve{h}(f - f_n), \tag{10}$$

$$\breve{v}'(f) = \breve{u}(f)\int_{-\infty}^{+\infty} \breve{h}(f_1)\delta(f - f_1 - f_n)\,\mathrm{d}f_1 = \breve{u}(f)\breve{h}(f - f_n). \tag{11}$$

The situation is different for sampled functions where the basband spectrum repeats with the sampling frequency $F_s = 1/T_s$. In this case, the baseband signal $u_s(t)$ and its Fourier transform $\breve{u}_s(f)$ are given by

$$\begin{aligned} u_s(t) &= u(t)T_s \sum_{\nu=-\infty}^{+\infty} \delta(t - \nu T_s), \\ \breve{u}_s(f) &= \int_{-\infty}^{+\infty} \breve{u}(f_1) \sum_{\nu=-\infty}^{+\infty} \delta(f - f_1 - \nu F_s)\,\mathrm{d}f_1 = \sum_{\nu=-\infty}^{+\infty} \breve{u}(f - \nu F_s). \end{aligned} \tag{12}$$

First, we proceed according to Eq. (7) and filter the periodic spectrum Eq. (12) with the baseband filter $\breve{h}(f)$. The result is then shifted to $f_\nu = f_n = nF_s$ by a mixing process. With a proper design of the baseband filter we pick the baseband signal spectrum $\nu = 0$, and the infinite sum reduces to one term,

$$\breve{v}_s(f) = \sum_{\nu=-\infty}^{+\infty} \breve{u}(f - \nu F_s - f_n)\breve{h}(f - f_n)\}^{\nu=0} = \breve{u}(f - f_n)\breve{h}(f - f_n). \tag{13}$$

Second, we shift the filter transfer function $\breve{h}(f)$ according to Eq. (8) numerically to $f_\nu = f_n = nF_s$, and then multiply with the periodic signal spectrum Eq. (12). Again, the infinite sum reduces to one term, if the shifted baseband filter is properly designed to select the signal spectrum at $\nu = n$,

$$\breve{v}_s'(f) = \sum_{\nu=-\infty}^{+\infty} \breve{u}(f - \nu F_s)\breve{h}(f - f_n)^{\nu=n} = \breve{u}(f - f_n)\breve{h}(f - f_n). \tag{14}$$

The calculations are visualized in Fig. 12. In the first case, Eq. (7) and Fig. 12(a), the filter cuts out the partial spectrum centered at frequency $f = 0$, and the mixing process shifts this partial spectrum by an integer multiple of the sampling frequency F_s. In the second case, Eq. (8) and Fig. 12(b), the filter is centered at an integer multiple of the sampling frequency F_s, and then cuts out the partial spectrum generated by the sampling process at this very frequency. Obviously, the two cases lead to the same final spectrum.

#206966 - $15.00 USD Received 27 Feb 2014; revised 21 Apr 2014; accepted 21 Apr 2014; published 29 Apr 2014

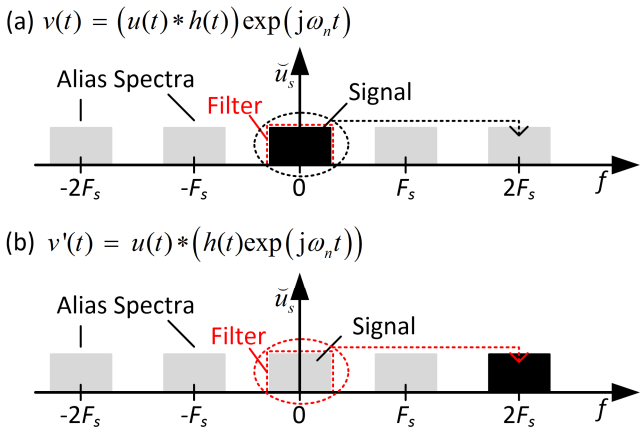

Fig. 12. Visualization of the equivalency of $v(t) = \left(u(t) * h(t)\right)\exp\left(\mathrm{j}\omega_n t\right)$ and $v'(t) = u(t) * \left(h(t)\exp\left(\mathrm{j}\omega_n t\right)\right)$ in the case of sampled signals. When a signal is sampled with the sampling rate F_s, the baseband spectrum repeats at integer multiples of F_s. (a) For the case of $v(t) = \left(u(t) * h(t)\right)\exp\left(\mathrm{j}\omega_n t\right)$ the signal is first filtered at baseband, resulting in the black partial spectrum. This is then shifted by a mixing process to the target frequency that is an integer multiple of F_s. (b) In the case of $v'(t) = u(t) * \left(h(t)\exp\left(\mathrm{j}\omega_n t\right)\right)$, the filter is first shifted to the target frequency at an integer multiple of F_s. The filter is then applied to the sampled signal and thus cuts out the (black) partial spectrum centered at the target frequency. The approaches (a) and (b) both yield the same result: The signal's baseband spectrum centered at the target frequency νF_s (here at $2F_s$).

Acknowledgments

This work was supported by the EU projects ACCORDANCE, OTONES, and FOX-C, the Agilent University Relations Program, the German BMBF project CONDOR, by the Karlsruhe School of Optics & Photonics (KSOP), and by the Helmholtz International Research School for Teratronics (HIRST). We further acknowledge support from Xilinx (XUP), Micram Microelectronic GmbH, Finisar, the Deutsche Forschungsgemeinschaft (DFG), and financial support from the Open Access Publishing Fund of the Karlsruhe Institute of Technology (KIT).

#206966 - $15.00 USD Received 27 Feb 2014; revised 21 Apr 2014; accepted 21 Apr 2014; published 29 Apr 2014